ORIGINAL ARTICLE

Cytometry PART A
Journal of the International Society for Analytical Cytology

A Statistical Pattern Recognition Approach for Determining Cellular Viability and Lineage Phenotype in Cultured Cells and Murine Bone Marrow

John Quinn,[1,2] Paul W. Fisher,[3] Renold J. Capocasale,[3] Ram Achuthanandam,[3] Moshe Kam,[4] Peter J. Bugelski,[1,3] Leonid Hrebien[4]*

[1]Department of Biomedical Engineering, School of Biomedical Engineering, Science and Health Systems, Drexel University, Philadelphia, Pennsylvania

[2]Treestar Inc., Ashland, Oregon

[3]Centocor Research and Development, Radnor, Pennsylvania

[4]Department of Electrical and Computer Engineering, College of Engineering, Drexel University, Philadelphia, Pennsylvania

Received 24 January 2006; Revision Received 23 March 2007; Accepted 4 April 2007

Grant sponsor: Centocor Research & Development, a wholly owned subsidiary of Johnson & Johnson Inc.

*Correspondence to: Leonid Hrebien, ECE Department Drexel University, 3141 Chestnut Street, Philadelphia, PA 19104

Email: lhrebien@cbis.ece.drexel.edu

Published online 31 May 2007 in Wiley InterScience (www.interscience.wiley.com)

DOI: 10.1002/cyto.a.20416

Abstract

Cellular binding of annexin V and membrane permeability to 7-aminoactinomycin D (7AAD) are important tools for studying apoptosis and cell death by flow cytometry. Combining viability markers with cell surface marker expression is routinely used to study various cell lineages. Current classification methods using strict thresholds, or "gates," on the fluorescent intensity of these markers are subjective in nature and may not fully describe the phenotypes of interest. We have developed objective criteria for phenotypic boundary recognition through the application of statistical pattern recognition. This task was achieved using artificial neural networks (ANNs) that were trained to recognize subsets of cells with known phenotypes, and then used to determine decision boundaries based on statistical measures of similarity. This approach was then used to test the hypothesis that erythropoietin (EPO) inhibits apoptosis and cell death in erythroid precursor cells in murine bone marrow. Our method was developed for classification of viability using an in vitro cell system and then applied to an ex vivo analysis of murine late-stage erythroid progenitors. To induce apoptosis and cell death in vitro, an EPO-dependent human leukemic cell line, UT-7_{EPO} cells were incubated without recombinant human erythropoietin (rhEPO) for 72 h. Five different ANNs were trained to recognize live, apoptotic, and dead cells using a "known" subset of the data for training, and a *K*-fold cross validation procedure for error estimation. The ANNs developed with the in vitro system were then applied to classify cells from an ex vivo study of rhEPO treated mice. Tg197 (human tumor necrosis-α transgenic mice, a model of anemia of chronic disease) received a single s.c. dose of 10,000 U/kg rhEPO and femoral bone marrow was collected 1, 2, 4, and 8 days after dosing. Femoral bone marrow cells were stained with TER-119 PE, CD71 APC enable identification of erythroid precursors, and annexin V FITC and 7AAD to identify the apoptotic and dead cells. During classification forward and side angle light scatter were also input to all pattern recognition systems. Similar decision boundaries between live, apoptotic, and dead cells were consistently identified by the neural networks. The best performing network was a radial basis function multi-perceptron that produced an estimated average error rate of 4.5% $\pm$ 0.9%. Using these boundaries, the following results were reached: depriving UT-7_{EPO} cells of rhEPO induced apoptosis and cell death while the addition of rhEPO rescued the cells in a dose-dependent manner. In vivo, treatment with rhEPO resulted in an increase of live erythroid cells in the bone marrow to 119.8% $\pm$ 9.8% of control at the 8 day time point. However, a statistically significant transient increase in TER-119^+ $CD71^+$ $7AAD^+$ dead erythroid precursors was observed at the 1 and 2 day time points with a corresponding decrease in TER-119^+ $CD71^+$ $7AAD^-$ Annexin V^- live erythroid precursors, and no change in the number of TER-119^+ $CD71^+$ annexin V^+ $7AAD^-$ apoptotic erythroid precursors in the bone marrow. A statistical pattern recognition approach to viability classification provides an objective rationale for setting decision boundaries between "positive" and "negative" intensity measures in cytometric data. Using this approach we have confirmed that rhEPO inhibits apoptosis and cell death in an EPO dependent cell line in vitro, but failed to do so in vivo, suggesting EPO may not act as a simple antiapoptotic agent in the bone marrow. Rather, homeostatic mechanisms may regulate the pharmacodynamic response to rhEPO.

ISAC International Society for Analytical Cytology

• **Key terms**
pattern recognition; flow cytometry; annexin V; 7-aminoactinomycin D; apoptosis; neural networks; anemia of chronic disease; erythropoietin

APOPTOSIS, or programmed cell death, is a highly regulated process involved in homeostasis. It is a transient state leading to cell death. Cells following the apoptotic pathway initially shrink in size, and then undergo chromatin condensation and membrane blebbing. Organelles are maintained until the late stages of apoptosis when the cell fragments and the debris are engulfed by phagocytes (1). Many functional markers associated with viability can be used to determine death-stage status of a given cell as measured by flow cytometry (2–12). One such marker for apoptotic cells is the protein annexin V, which binds phosphatidylserine (PS), a lipid maintained in greater proportion on the inner leaflet of the cellular membrane in live cells. Early in apoptosis, PS is redistributed to the outer leaflet of the cellular membrane, resulting in an increase in annexin V binding sites, and a means to distinguish live cells from apoptotic cells (6). The dye 7-aminoactinomycin D (7AAD) is another cell viability marker. In dying cells, loss of cellular membrane integrity allows for unrestricted access of 7AAD to nuclear DNA, resulting in an increase in 7AAD binding, and a means of identifying dead cells (7). Forward laser light scatter (FSC) and side or 90° laser light scatter (SSC) are parameters correlated to cell size and granularity, respectively, and can be used as indicators of the morphological changes that cells undergo during apoptosis (1). It has been reported that cell shrinkage and loss of granularity, detectable by light scatter measurement, can precede PS redistribution in the apoptotic process and can be used to discriminate the earliest apoptotic cells in some cases (13).

A method for classifying cells by viability proposed by Lecoeur et al., uses dual staining with annexin V and 7AAD to create a two-dimensional space that maps to viability (7). Intensity thresholds are set for both markers to produce boundaries or "gates," which separate live, apoptotic, and dead cells. The boundaries separate cells "positive" for 7AAD as dead, and cells "positive" for annexin V but "negative" for 7AAD as apoptotic. Cells "negative" for both markers constitute the live population. However, the boundaries are often set in a somewhat subjective manner, and run parallel to the annexin V and 7AAD intensity axes (7,12,13). The result is that classification of individual cells, particularly near the gate boundaries, varies between experts.

Since intensity values vary with experiment, animal, photomultiplier amplification, compensation, and the combination of fluorochromes, setting a threshold to differentiate "negative" and "positive" requires consideration of multiple variables, and often depends on the experimenter's experience. Additionally, molecular mechanisms regulating staining with many of the vital dyes in living and apoptotic cells are not well understood. It is known that 7AAD inserts stochiometrically between cytosine and guanine bases in DNA allowing for its use in detecting damaged membranes, but the process that regulates its passage across the cellular membrane is unknown (5). This situation adds to the difficulty in interpreting cells with intensity below the 7AAD binding saturation point that occurs when the dye is able to freely cross a damaged membrane. There are also no visual data analysis methods that handle four parameters simultaneously, which would allow for consideration of 7AAD, annexin V, FSC, and SSC. Because of these factors there are regions in the decision space that are difficult to classify and experts disagree on where decision thresholds should be set (3–12).

Described in this study are the development and application of an objective method for classification of cellular flow cytometric data, using artificial neural networks (ANNs). The method was developed for classifying cellular viability as live, apoptotic, or dead using an in vitro data set. Once validated, we applied the ANN approach to test the hypothesis that erythropoietin (EPO) inhibits apoptosis and cell death in erythroid precursor cells in vivo. AntiTER-119 binds a glycophorin-A associated protein, and has been used to discriminate erythroid precursors from other bone marrow cells in mice. The expression of CD71 (transferrin receptor) is inversely correlated with maturation of erythroid precursors (14,15). To test this hypothesis it was necessary to identify erythroid cells (Ter-119+) from bone marrow and roughly determine their stage of differentiation (CD71 levels), so in addition to classifying events by viability ANNs were used to classify for lineage and developmental stage.

An ANN (16–22) is a weighted directed graph where the nodes are artificial neurons, and weighted directed edges connect neuron outputs with neuron inputs. In this study, we considered both feed forward networks in which the graphs have no feedback loops (multilayer perceptrons and radial basis function networks) and feedback loop, or recurrent, networks (recurrent multilayer perceptron, competitive learning network, and Kohonen's self-organizing maps). The inputs to the ANNs were cellular intensity measures collected using flow cytometry. The collected parameters for viability determination were annexin V FITC and 7AAD intensity, along with forward angle scattered light (FSC) and side angle scattered light (SSC). For erythroid lineage and developmental stage identification, TER-119 PE and CD71 APC were used. ANNs were induced to develop input–output maps through supervised learning, with the exception of the self-organizing map which learns in an unsupervised manner. The ANNs trained through supervised learning were provided a set of inputs with a corresponding set of desired outputs, called a training set. The networks classified these events based on their pattern of measured intensities, and then this output was compared to the desired ("correct") classification to elicit modification of the architecture (e.g., weight changes in a multilayer perceptron) so as to produce the correct answer from the network. Training sets were obtained by identifying intensity patterns in our selected input parameters that have been classi-

fied consistently in the literature as corresponding to one of the biological states we are seeking to identify, and selecting the events in our collected data that match these patterns. Network performances were compared on the basis of several error criteria; the correct classification of events of known class that have not been previously shown to the networks, and a comparison of classification of the complete set of events to an expert method (7). Additionally, we measured the classification consistency, or repeatability, of each type of network. Twenty replicates of each network were created, each trained with a unique training set, and the consistency of classification per event for twenty replicates was calculated.

Materials and Methods

Reagents

rhEPO was obtained from Ortho Biologics (Raritan, NJ). Doses are expressed as IU/kg (The activity of rhEPO was 120 IU/ug.). The following monoclonal antibodies (mAbs) against murine cell surface markers were purchased from BD-Pharmingen (BD Biosciences, San Jose, CA): PE-conjugated anti-TER-119; biotinylated antiCD71 (clone C2), APC-conjugated streptavidin; FITC conjugated annexin-V, and the viability/DNA probe 7AAD. Appropriately labeled isotype-matched IgG controls were also used.

In Vitro Experiments

UT-7_{EPO} cells, an EPO dependent subline of UT-7 human megakaryoblastic leukemia cells (23), were a gift of Dr. Francis Farrell (Johnson and Johnson Pharmaceutical Research and Development) and were maintained in Iscove's modified Dulbecco's medium (IMDM) supplemented with 1 IU/mL rhEPO and 5% fetal bovine serum. For analysis of apoptosis, the cells were pelleted by centrifugation and were resuspended in 2 mL of IMDM medium supplemented with 5% FBS. Cells were pre-incubated without rhEPO for 24 h and then were seeded at 5×10^4 cells/well in 12-well plates in the absence or presence of rhEPO (0.01, 0.03, 0.1, 0.3, or 1.0 U/mL), incubated at 37°C for an additional 48 h, transferred to flow cytometry tubes, washed, and incubated for 15 min with 5 μL each of annexin-V and 7AAD (in 100 μL of annexin-V binding buffer). Three replicates were analyzed for each of five doses and control, producing a total of 18 samples. After incubation, the tubes were immediately analyzed by 2 color flow cytometry as described previously (Bugelski PJ, Nesspor T, O'Brien J, Makropoulos D, Shamberger K, Fisher PW, James I, Capocasale RJ. 2005. Pharmacodynamics of recombinant human erythropoietin in normal mice: Effects of a single dose on cell cycle, apoptosis and maturation of late stage erythroid precursors. Manuscript submitted for publication).

In Vivo Experiments

Nine week old heterozygous female Tg197 transgenic mice were obtained from Ace Laboratories (Boyertown, PA). Founder mice for this colony were obtained from G. Kollias and have been described previously (24). We have shown previously that Tg197 mice are a model of anemia of chronic disease and express increased levels of apoptosis in their medullary erythroid progenitor compartment (25). Mice were acclimated for at least 2 weeks and group housed with a 12 h light/dark cycle. Food and water were provided *ad libitum*. Groups of mice (8/group) received a single subcutaneous injection of 10,000 U/kg rhEPO or phosphate buffered saline 1, 2, 4, or 8 days prior to collection of bone marrow or blood. Four groups of eight mice produced a total of 32 samples. In Tg197 mice, this dose of rhEPO has been shown to cause a 2.6-fold increase in peripheral blood reticulocytes 4 days after a single subcutaneous injection (data not shown). All mice were maintained in the pathogen-free animal facility at Centocor, Radnor, PA. The Centocor Animal Care and Use Committee approved all procedures. Femoral bone marrow was obtained by flushing both femurs and mechanical dispersion. Marrow was analyzed without being subjected to hypotonic lysis. Cells were suspended in phosphate buffered saline (PBS) without Ca^{++} or Mg^{++} and supplemented with 2% heat-inactivated fetal calf serum (FCS) and 0.1% NaN_3 (staining buffer). Cells were maintained on ice and protected from light during antibody labeling with centrifugation steps performed at 4°C. Cells were aliquoted into 96-well polystyrene round bottom tissue-culture plates at 5×10^5 per well and pre-incubated with antimurine CD16/CD32 (FcgRIII/II) 2.4G2 to reduce FC receptor-mediated antibody binding. Following Fc block, cells were incubated for 20 min with panels of rat antimurine monoclonal antibodies to TER-119 and CD71 to delineate erythroblasts. Erythroid phenotyped cells were stained with FITC- labeled annexin V and 7-AAD as per manufacturer's instructions. All samples were analyzed immediately following the staining procedures.

Flow Cytometry

Samples were analyzed on a FACSCalibur flow cytometer (BD Biosciences, San Jose, CA) equipped with a 15 mW air-cooled 488 nm argon ion laser for excitation of FITC, PE, and 7AAD and a 635 nm diode laser for excitation of APC. Photomultiplier tube voltage and spectral compensation were established using cells single-stained with FITC alone, PE alone, 7AAD alone or with streptavidin APC alone. FITC, PE, 7AAD, and APC fluorescence were acquired on 4-decade log scales. All parameter measures were then partitioned into 1,024 uniform channels and recorded as dimensionless intensities. Measurements for at least 10,000 cells were made per sample, with the measurements obtained from a cell termed an event, and sample used in this study to refer to all events collected from a single animal. Data were collect in FCS format as matrices with each row representing an event and each column a parameter. Each event is thus described by a vector of intensity values, a single row from the matrix.

Data Analysis

Data were exported to Matlab® version 6.5 software (The Mathworks, Natick, MA) for processing. Data were grouped by data set, with the term data set used here to describe the set of samples from a given experiment. On a sample by sample basis, cell fragments and doublets were excluded mathemati-

Table 1. Description of applied ANNs

ARTIFICIAL NEURAL NETWORK	ACRONYM	OPERATING STYLE	LEARNING STYLE	NO. OF LAYERS	ACTIVATION FUNCTION(S)
Multilayer perceptron	MLP	Feed forward	Back propagation	3	Sigmoid & Unit step
Radial basis function multi-perceptron	RBFP	Feed forward	Back propagation	3	Radial & Unit step
Recurrent multi-perceptron	RMP	Recurrent	Back propagation	3	Sigmoid & Unit step
Learning vector quantization	LVQ	Recurrent	Hybrid of competitive & back propagation	3	Competitive & Unit step
Self organizing map	SOM	Recurrent	Competitive	2	Competitive

cally by removing all events with FSC or SSC intensity values measured in the maximum channel, and fluorescent intensities were normalized to a unit scale. We applied five different ANNs, which are available in the Matlab neural network toolbox, to develop decision rules for flow cytometry data classification. The ANNs were: a multilayer perceptron (MLP), a radial basis function perceptron (RBFP), a recurrent multi-perceptron (RMP), a learning vector quantization network (LVQ), and a self-organizing map (SOM). Table 1 lists each of the five networks and their main features. An example of a three layer MLP is illustrated in Figure 1. Details of the other networks used in this study are available in the literature (16–22). The three layer MLP consists of an input layer of four (4) neurons, a hidden layer of three (3) neurons and an output layer of three (3) neurons. The 4-dimensional input $[x_1 \ x_2 \ x_3 \ x_4]$ is of single event intensity values for the parameters FSC, SSC, 7AAD, and annexin V. The j^{th} neuron in the hidden layer ($j = 1, 2, 3$) has the input net_j, which is a weighted sum of the input intensity values:

$$\text{net}_j = \sum_{i=1}^{4} x_i w_{ji} + w_0 \tag{1}$$

where the weights w_{ji}, and the bias w_0 (an additive weight that can be used to set a reference point of operation) are tunable real numbers.

The output of the j^{th} neuron in the hidden layer is then:

$$y_j = f(\text{net}_j) \tag{2}$$

where the continuous function $f(\bullet)$ is known as the activation function and is often selected as a saturation function (sigmoidal or logistic function) or as a unimodal concave down function (e.g., Gaussian). In this study, we have selected a sigmoidal activation function for the multilayer perceptron of the form:

$$f(x) = \frac{1}{1 + \exp(-x)} \tag{3}$$

The input to the k^{th} ($k = 1, 2, 3$) neuron in the output layer is:

$$\text{net}_k = \sum_{i=1}^{4} y_i w_{ki} + w_0 \tag{4}$$

and the output Y_k of the k^{th} neuron in the output layer is then:

$$y_k = f(\text{net}_k) \tag{5}$$

The output is a label that classifies the input into one of three categories. Proper mapping of the input to the output is achieved by adjusting the connecting weights during the process of training. Here we have used the popular back propagation algorithm (22), where the network weights are updated in proportion to the classification error, magnitude of the output, and a user defined proportionality constant η, called the learning rate. For the weights w_{jk} connecting the j hidden neurons to the k output neurons the updating proportions, called delta values, are calculated as:

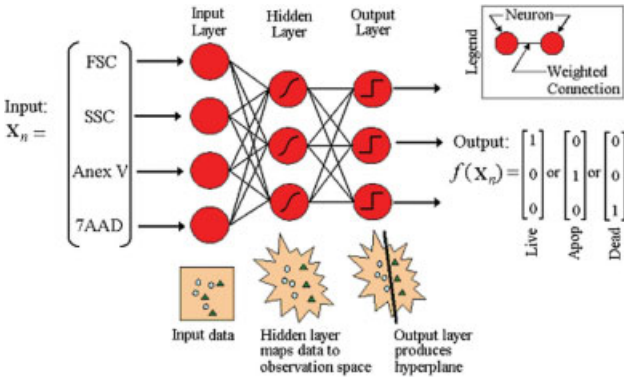

Figure 1. Illustration of a three-layer feed forward multilayer perceptron for viability classification. Neurons are pictured in red, and the black lines between neurons represent weighted connections. Below each neuron layer is graphical representation of the network affect on input data. Circles and triangles represent two classes of data. The input layer of neurons accepts Xn, a four dimensional vector, composed for viability classification of FSC, SSC, Annexin V, and 7AAD intensities. The input data is plotted below the input layer in two-dimensions and cannot be separated by a hyperplane. The hidden layer of neurons accepts a weighted sum of the inputs and through activation functions, maps the data into an observation space. A two-dimensional projection of the observation space is shown below the hidden layer, in which the data are transformed to be separable by a hyperplane. The output layer of neurons produces a hyperplane that separates the two classes. This hyperplane is illustrated below the output layer, separating the transformed data. The output of the network, f(Xn), is a vector of binary numbers indicative of class. For classification by viability as shown here, the classes are live, apoptotic, or dead.

$$\delta_k = f'(\text{net}_k)[t_k - y_k] \quad (6)$$

where t_k is the target output, and $f'(\bullet)$ is the derivative of function $f(\bullet)$. For the weights w_{ij} in the preceding layers the delta values are computed by propagating the error backward, producing:

$$\delta_j = f'(\text{net}_j) \sum_j w_{jk}\delta_k \quad (7)$$

Weights connecting consecutive layers, termed layer L and layer M, are then updated by:

$$\Delta w_{\text{LM}} = \eta \delta_{\text{M}} y_{\text{M}} \quad (8)$$

The process of data presentation and weight updating continues to cycle until a stopping criterion is met. The result of network training is the creation of a set of hyperplanes that separate the input data according to class—in four dimensions in our case. Collectively these hyperplanes are referred to as decision boundaries.

Training Data Selection Using Expectation Maximization (EM) Algorithms

Each ANN was trained using a set of 500 cells collected from a pool of training data. The composite training data were selected and removed from the complete data set using EM algorithms. Figure 2(a) shows a scatter plot of data from the in vitro study of parameters 7AAD versus annexin V (sub-Fig. 1), with the distribution of the intensity values of each parameter shown along the corresponding axis (sub-Figs. 2 and 3). Several recent studies have identified three consensus classification regions as annexin V^{low} and $7AAD^{low}$ (live cells), $7AAD^{low}$ with annexin V^{high} (apoptotic cells), and $7AAD^{high}$ (dead cells). However, the boundaries or gates that separate "high" and "low" have been defined subjectively based on author experience (2–12). A panel of experts was used to classify the data as live, apoptotic or dead. Even though there was variability in the assignment of the events at the boundary, there was general consensus on the class of the majority of events. These regions of consensus corresponded closely to the peaks of the univariate distribution of the 7AAD and annexin V intensities. On the basis of the biology of these two parameters we have modeled the intensity values of both 7AAD and annexin as bimodal distributions, with a "low" intensity region and a "high" intensity region. Univariate distributions were produced by a Gaussian mixture model rather than bivariate Gaussian distributions to account for the biology of the markers. The expectation maximization (EM) algorithm was applied to individual parameters to create a model of the data. The EM algorithm uses Bayesian estimation to iteratively improve the statistical model of a data set (26). Populations within flow data are assumed to have normal distributions using arguments based on the central limit theorem (the cardinality of the data is large), so we have used a normal basis for our models (27).

EM algorithms were initialized to have two populations, or components, for each parameter (e.g., 7AAD or annexin V intensity), and randomly generated means and covariance. The metric for goodness of fit was the log likelihood of membership for all events and all components. Stopping conditions were log likelihood improvement of less than one percent in consecutive iterations, instituted after the tenth iteration. The algorithm was required to perform at least ten iterations to prevent the identification of local minima as the best fit. Ten iterations of the EM algorithm were chosen as a minimum requirement because the probability of a large (an order of magnitude) improvement in log likelihood became insignificant (0.05) at that point, with significance experimentally determined using the in vivo data set. To select events for use as a viability training set, the EM algorithm was applied to each sample three times. Initially the 7AAD intensity values of all events were provided as input, and the EM algorithm was used to create a bimodal distribution, with the two modes assumed to be "not dead" (live or apoptotic) and dead populations. Figure 2(a)-2 shows this distribution as the solid line above the 7AAD axis of a scatter plot (Fig. 2(a)-1) from an in vitro sample. The second application of the EM algorithm excluded the events identified thus far as dead, and was used to create a bimodal distribution of the annexin-V intensity values, with the two modes assumed to be live and apoptotic populations. This distribution is shown in Figure 2(a)-3 adjacent to the annexin V axis. The result of the first two applications of the EM algorithm was to separate the dead events based solely on 7AAD intensity, and to separate live and apoptotic events from the "not dead" population based on annexin V intensity. The third application of the EM algorithm completed the models of the live and apoptotic populations by fitting unimodal normal distributions to the 7AAD intensities of each of these two classes. Figure 2(a)-2 shows the apoptotic events 7AAD intensity model distribution as a dashed line overlaid with the model of the complete sample. The live events 7AAD distribution is not pictured as it overlaps substantially with the "not dead" mode of the complete sample distribution.

Upon completion of modeling, training data for the neural networks were selected from within one standard deviation of the mean of each population to acquire training data that represents the most common examples of each class. In Figure 2(a)-1 the overlaid boxes indicate the ranges that were identified as being of unquestioned as to class, and acceptable for selecting training data from. The lower left box identifies live cells, the upper left box identifies apoptotic cells, and the right hand box identifies dead cells.

Bimodal models created with the EM algorithm were also used to select training data for classification of events by lineage and developmental stage. On the basis of the work of Socolovsky et al., Kina et al., and Chang et al., the parameters Ter119 and CD71 were used to identify events representative of two developmental stages of erythroid precursors (14,15,28). Two applications of the EM algorithm were required to create the necessary training sets, with the first

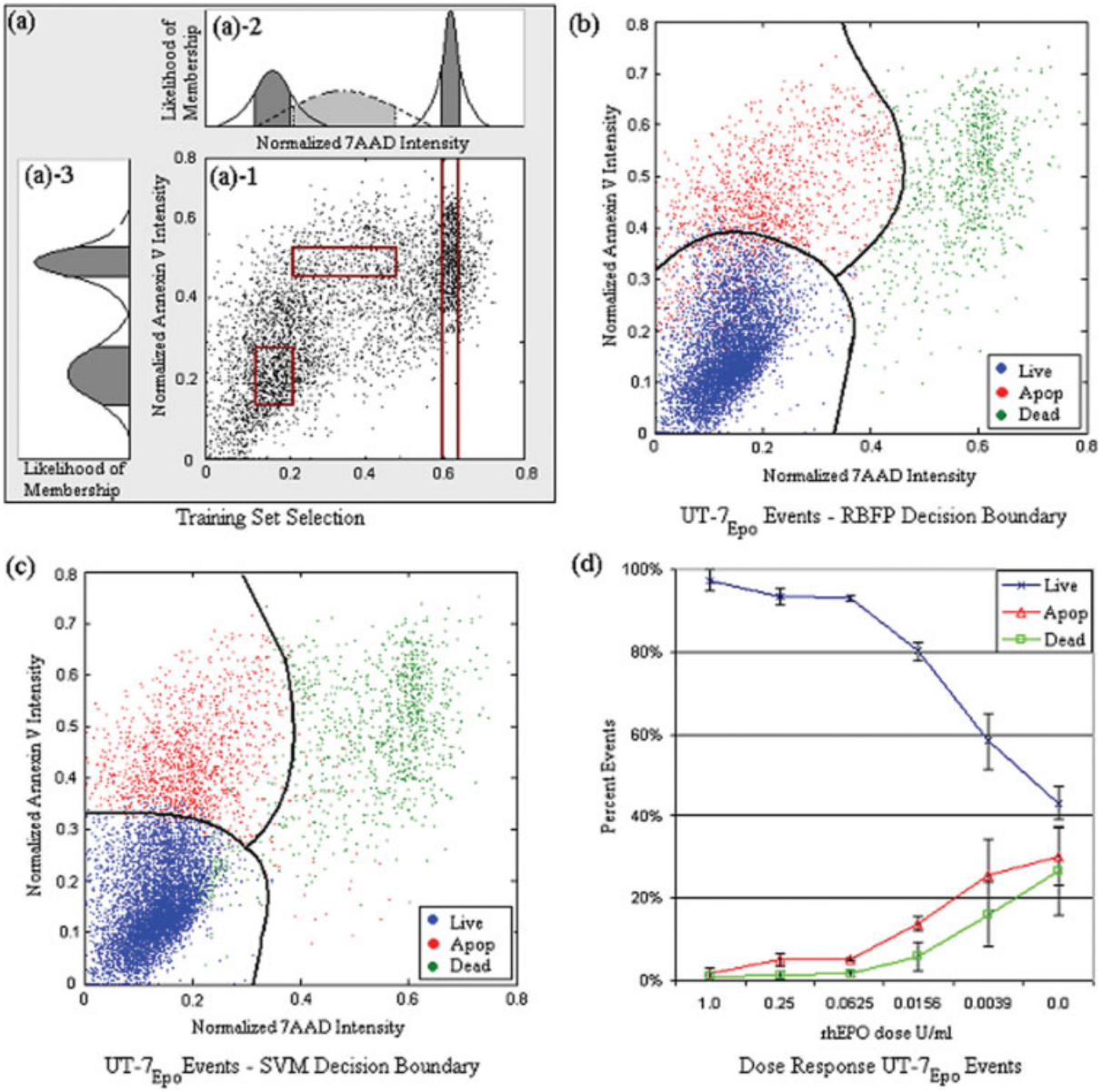

Figure 2. Experimental results using UT-7EPO cells. (**a**) Illustration of the training data selection process. In (**a**)-1 one UT-7EPO sample is plotted for the parameters 7AAD and annexin V. The EM algorithm created model of the distribution of 7AAD intensity is shown as a solid line in (**a**)-2 with one standard deviation of each population shaded gray. This model was used to identify not-dead and dead events. The model of annexin V intensity is shown in (**a**)-3, used to separate live and apoptotic events from the not-dead population. In (a)-2 completion of the apoptotic population modal is shown as a dashed line. After the not-dead population was separated the 7AAD intensity of each population was modeled. Using these models events were for training from the boxes shown in (a)-1 as live (lower left), apoptotic (upper left) and dead (far right). (**b**) Two-dimensional representation of the four-dimensional decision boundary created by the RBFP. Blue colored cells were classified ''live,'' red were classified ''apoptotic'' and green were classified ''dead.'' (**c**) The two-dimensional approximation of the SVM decision boundary. Its shape closely resembles the RBFP boundary. (**d**) Concentration response results from UT-7EPO study, with cell classification made by radial basis function perceptron. With decreasing levels of rhEPO we observe increased apoptosis and cell death.

application used to model events positive and negative for TER-119, which are erythroid and nonerythroid (NE) events respectively. The second application was used to model CD71 positive and negative events, late precursors and very late precursors to red blood cells, respectively. In this work the term late precursor (LP) is used to indicate cells that would be classified as proerythroblasts, basophilic erythroblast, and possibly polychromatic erythroblasts by the gating system described in (14). Very late precursors (VLP) include polychromatic and orthochromatic erythroblasts as classified by the same expert method.

To minimize animal to animal differences, compensation variations, and amplification variability, the EM algorithm was used to create a model for each data set. The models were then

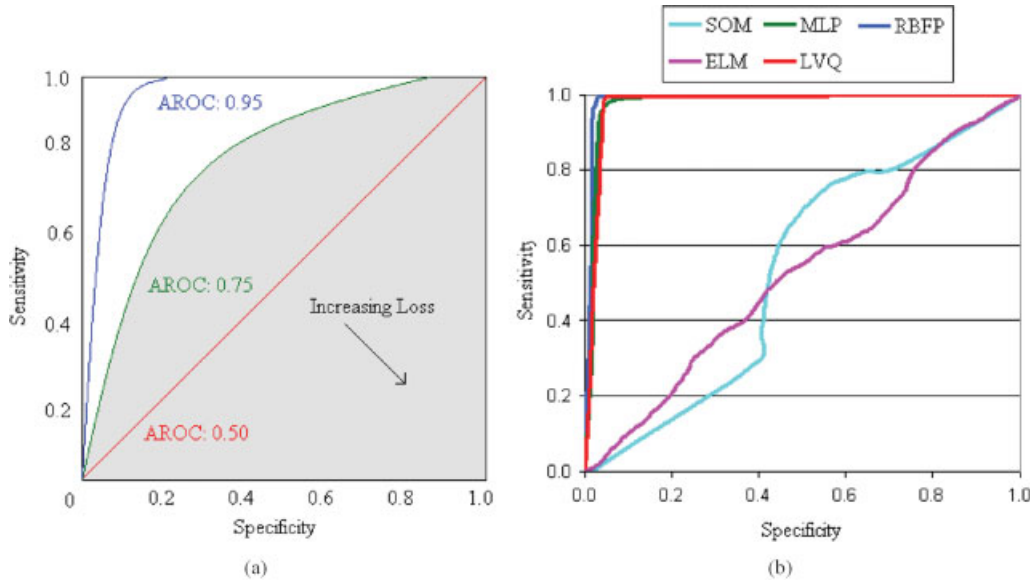

Figure 3. (**a**) Receiver operating characteristic curve (ROC) illustration. An ROC is a plot of the rate of correct classification (sensitivity, *y*-axis values) versus the incurred rate of misclassification (specificity, *x*-axis values). Coordinates on the plot are called operating points and are produced by plotting the classifiers sensitivity versus specificity while varying the cost of misclassification. In this example three lines are plotted; the red line is the performance of a random classifier. The green line is classifier that performs better than random. The blue line is a representative example of the best performing networks we have tested. The statistic reported is area under the ROC curve (AROC). AROC is calculated by numerically integrating an ROC curve. The region shaded gray is the area under the green curve. Accompanying each ROC curve in the figure is the AROC value. (**b**) ROC curves for each ANN. Each curve shown is the average of the three possible two-way comparisons per type of ANN, The sensitivity and specificity for each two-way comparison was calculated as the average of twenty iterations of each type of ANN.

used to label each event as live, apoptotic, dead, or unknown (all events with intensity values outside the training candidate ranges). An equal number of event intensity vectors were then taken from each sample, pooled, and randomly distributed into twenty-one training sets, with 500 events each, containing live, apoptotic, dead and unknown examples. An additional data set of 500 events was created by random selection from the pooled data for use with the MLP and RMP during training. This additional set or "termination set" was used later in the process to determine the stopping conditions for these two networks.

During training, events labeled as "unknown" were omitted. These events were used for comparing classification results versus an expert system and for calculating the consistency of repeated classifications by replicates of each type of ANN. Network training and error estimation were implemented using a *K*-fold cross validation format.

Viability Analysis by the Expert (Expert Method)

A panel of experts performed the classification of events in our data sets according to the method proposed by Lecour et al. (7). The classification results generated by the ANNs were compared to the classification generated by this panel of experts and are reported in Table 2 as the percent disagreement with expert.

K-fold Cross Validation

Cross validation is a means of estimating a classifier's accuracy by holding back a portion of the available training data for use as testing data. In *K*-fold cross validation the training dataset is divided randomly into *K* mutually exclusive subsets (folds) of approximately equal size. A classifier is trained and tested *K* times by excluding one fold from training each time, applying the resulting classifier to the excluded fold, and then calculating the error. The cross validation estimate of accuracy is the number of correct classifications divided by the number of instances in the dataset. We have followed the work of Kohavi (29) and divided the training data into twenty-one folds ($K = 21$) of 500 events each. Twenty of the folds were used in the cross validation process resulting in the creation of twenty ANNs for each type of network. The expected error for each type of ANN was reported as the average error produced by the twenty networks. Additionally, the twenty-first data set was used to determine the consistency of the twenty networks created for each ANN type. This data set was presented to each of the twenty ANNs per type, and all events were classified. The percentage of events that were not assigned to one class exclusively by all twenty networks was reported as percent varying.

Receiver Operating Characteristic (ROC) Curves

The classification performance of the ANNs was compared to the expert method. The comparison metric used is

Table 2. Performance indices of UT-7EPO cells using five different artificial neural networks and an SVM

ALGORITHM	EXPECTED ERROR	PERCENT VARIYING	AROC	PERCENT DISAGREEMENT WITH EXPERT
RBFP	(4.5 ± 0.9)%	2.2%	0.99 ± 0.01	(6.4 ± 1.3)%
MLP	(3.4 ± 1.6)%	15.2%	0.96 ± 0.02	(7.8 ± 2.5)%
LVQ	(6.0 ± 1.3)%	24.4%	0.96 ± 0 01	(15.3 ± 2 2)%
SOM	(25.3 ± 4.3)%	26.8%	0.69 ± 0.17	(37.2 ± 3.2)%
RMP	(33.2 ± 28.8)%	60.1%	0.64 ± 0.22	(30.0 ± 29.3)%
SVM	(3.6 ± 0.9)%	12.8%	0.98 ±0.01	(9.4 ± 2.8)%

the area under the Receiver Operating Characteristic (ROC) curve. A ROC curve is a means of characterizing the performance of a binary classifier. Good classifiers minimize loss, a weighted sum of the classifier's probability of missed detection and the probability of false alarm. For binary classification, loss L for an object of class c is often expressed as:

$$\text{Loss} = \lambda_{21} p(c_2)\epsilon_2 + \lambda_{12} p(c_1)\epsilon_1 \tag{9}$$

where λ_{nm} is the cost of misclassifying a data point of class n to class m, $p(c_n)$ is the frequency or *a priori* probability of a data point being of class n, and ϵ_n is the probability of misclassifying a data point belonging to class n. A ROC curve is created by plotting the classifier's sensitivity $(1 - \epsilon_1)$ on the vertical axis against its specificity (ϵ_2) on the horizontal axis, while varying either the *a priori* probability of the null hypothesis or the misclassification cost to create multiple operating points (30). Example ROC curves with the associated area under the ROC (AROC) are shown in Figure 3(a), with the direction of increasing loss indicating increasingly poor performance. Perfect classification would produce an AROC of 1.0. Random classification yields an AROC of 0.5. In this study, the misclassification cost λ_{nm} has been varied from 0 to 1, at intervals of 0.1, and used to calculate ROC operating points. For example, an ANN calculates the probability that an event represented by intensity vector $\boldsymbol{x}$ belongs to c_1 and assigns the vector to c_1 if $p(c_1|\boldsymbol{x}) > \lambda_{21}/(\lambda_{12} + \lambda_{21})$, a measure of the cost of misclassification. By varying λ_{12} and λ_{21}, sensitivity and specificity of the classifier was calculated for a range of misclassification costs. ROC curves were created by plotting the sensitivity versus specificity for each of these operating points.

The ROC curves have been integrated numerically and the scalar metric AROC calculated. By using AROC as a metric we account for classifier performance at multiple operating points without having to specify the cost, which in practice is unknown. To accommodate three possible outcomes (live, apoptotic, dead) we used three ROC curves, one for each possible pair wise comparison, namely live versus apoptotic, live versus dead, and apoptotic versus dead. ROC curves showing the average of the three possible pair wise comparisons are shown in Figure 3(b) for all ANNs. Each of the three AROCs are calculated and then averaged to create a score for the classifier.

Additionally, in our results we report the percentage of events that were classified differently by the ANN versus the expert approach at equal error costs as a more intuitive measure. This metric is reported as "percent disagreement with expert" in Table 2.

Support Vector Machines (SVMs)

The final measure of network success employed was a comparison of the ANN decision boundaries to another pattern recognition technique for the purpose of comparing our results against a different pattern recognition algorithm. Support vector machines (SVMs) are popular and complementary pattern recognition algorithm to ANNs and have previously been demonstrated to be applicable to cell classification from an in vitro flow cytometric data set (31) SVMs are discrete algorithms that can be used to find the maximum margin between classes of data for the purpose of separating the data by class (17). For a training set $\mathbf{x}$, with weights w, bias b and classification values $y_i \in \{-1, 1\}$ used to separate two classes n and m, SVM training is a minimization problem with the constraints:

$$x_i \cdot w + b \geq +1 \quad \text{for} \quad y_i = +1(\text{class } n) \tag{10}$$

$$x_i \cdot w + b \leq -1 \quad \text{for} \quad y_i = -1(\text{class } m), \tag{11}$$

of the function:

$$f(\mathbf{x}) = \text{sign}((\mathbf{x} \cdot \mathbf{w}) + b) \tag{12}$$

In concept, minimizing f with respect to this constraint finds the location of the hyperplane directly between the positive and negative training sets. The training points that lie on the hyperplanes at each edge of the margin are called support vectors. Data that cannot be directly separated by a hyperplane can be mapped to a space of higher dimensionality where separation is possible. Mapping was implemented though a nonlinear transformation of the data, specifically with a Gaussian function that transformed pattern x to pattern $z = \varphi(x)$ using:

$$\varphi(x) = \frac{\exp(-x^2)}{\sqrt{2\pi}} \tag{13}$$

SVMs are limited to differentiating data from two classes. To accommodate three classes a "one against all" approach was

applied. This format trains three different binary classifiers, each one trained to distinguish the examples in a single class from the examples in all remaining classes. When it is desired to classify a new example, all three classifiers are implemented and the classifier which provides the largest value of output is chosen. "One against all" is a powerful scheme, producing results that are usually at least as accurate as other methods designed to accommodate more than two classes (32).

Pattern Recognition Application

For all five networks listed in Table 1 the inputs were four-dimensional vectors of intensity measures for the parameters FSC, SSC, 7AAD, and annexin V. Input values were normalized to range from zero (0) to one (1). For each type of ANN, twenty networks were created, each using a separate 500 event training set. Roughly half of the events in each training set were of "known" class and were used for training, while the other half were of "unknown" class and were used only to test classification consistency. Network weights and biases were initialized randomly, and a learning rate of 0.05 was used.

MLPs and the RMPs were each configured to have four (4) input neurons, connected to three (3) hidden neurons, and three (3) output neurons. The number of hidden neurons was chosen following the recommendation of Duda, Hart and Stork (9) to set the total number of free parameters (weights) equal to one tenth of the number of degrees of freedom in the system (number of events in the training set). Three hidden neurons caused the network to have 24 total weights, for roughly 250 events in the training set. Hidden layer neurons were given sigmoidal activation functions shown in equation 3. Output layer neurons had unit step activation functions of the form:

$$f(x) = u(x-b), \begin{cases} x-b \geq 0 & f(x)=1 \\ x-b < 0 & f(x)=0 \end{cases} \tag{14}$$

with bias b. Outputs were either {1 0 0} for live events, {0 1 0} for apoptotic events or {0 0 1} for dead events. Network weights were updated at the end of each epoch, which is one complete presentation of the training data. Each network was allowed to iterate through 25 epochs, with an early termination option. Early termination occurred if at the end of an epoch, the ANN classified the events of known viability within the "termination set" with 98% accuracy. Training examples were presented to the MLP in random order. For the RMP, training examples were ordered spatially by nearest neighbor in the 7AAD versus annexin V plane, using the two dimensional origin as a starting location, and Euclidean distance between events as a measure of proximity. The events were then presented to the RMP in this order so that for each event the class of the nearest neighbor (the previously presented event) would be used as a factor in classification through the feedback connection.

The RBFP, LVQ and SOM are all one-pass networks, meaning that the training data were shown to the network only once. RBFPs were configured in the style proposed by Broomhead and Lowe (33) with four (4) input neurons, one (1) hidden neuron for each training data point with a radial basis activation function, and three (3) output neurons with linear activation functions. The radial basis activation function was of the form:

$$f(x) = \exp(-x^2) \tag{15}$$

and the linear function is:

$$f(x) = wx + b \tag{16}$$

The width of the radial basis functions was calculated as described in Ref. 21. Each output unit implemented a linear combination of these radial basis functions. Conceptually, this network used the training examples to interpolate a mapping of input to output classification for the complete input space.

SOM networks are competitive learning networks that define a spatial neighborhood for each output neuron (22). SOM networks were configured to have four (4) input neurons, no hidden neurons, and three (3) output neurons. The output neurons used competitive activation functions; functions with an output magnitude inversely proportional to the similarity of input x and the output neuron weights w_i. The output neuron that is most similar to the input produces that largest output and is declared the "winner". Euclidean distance was the metric used to define similarity, making the competitive activation function:

$$f(x) = \min_{i=1:N} \|x - w_i\| \tag{17}$$

where N input neurons are represented by weights $w_{1:N}$, and $\alpha f(x)$ is the quantity the winning neuron is updated by. The constant α is known as the learning rate, a modifier used to reduce the update amount to a fraction of the distance between input pattern x and neuron i. A learning rate of $\alpha = 0.1$ was used in this work. During classification, the network weights were immutable. A winning neuron was determined for each input event, and the event was assigned to the class of the winning neuron.

The LVQ networks had four (4) input neurons, nine (9) hidden neurons, and three (3) output neurons. The hidden neurons had competitive activation functions as defined in equation 17 and created groupings of the inputs using unsupervised learning. Each output unit implemented a linear combination of the competitive neurons using the linear activation function defined in equation 16. Through supervised learning, the output layer was induced to develop a mapping that combined the nine (9) sub-populations created by the hidden layer into the three (3) target populations by grouping the sub-populations in the manner that produced the fewest misclassifications.

Results

The eighteen sample in vitro experiment was used to test the applicability of ANNs to classifying flow data. Figure 2 and Table 2 document the in vitro results. Figure 2(b) shows a

two-dimensional projection of the decision boundary created by the RBFP where events classified as live are shown in blue, events classified as apoptotic in red, and events classified as dead in green. In the figure, overlapping classes are visible particularly on the border between live and apoptotic events because this is a two-dimensional projection of a four-dimensional decision boundary. The overlapping classifications in the 7AAD and annexin V plot indicate that FSC and SSC were factors in constructing the decision boundaries. Figure 2(b) is representative of the boundaries produced by the various ANNs and their performance metrics are listed in Table 2 with their standard deviations. The four performance metrics were described in the Materials and Methods section and are again listed here: expected error (calculated during cross-validation), percent varying (events that were not classified uniformly by twenty ANNs of a given type), AROC (comparison of ANN results to an expert method), and percent disagreement with expert (events classified differently by the ANN and the expert at equal misclassification costs). The RBFP, LVP, and MLP all produced expected error rates of 6% or less, with RBFP being the best performer with an expected error of 4.5% $\pm$ 0.9%, 2.2% of the events varying, AROC of 0.99% $\pm$ 0.01%, and 6.4% $\pm$ 1.3% of the events disagreeing with expert classification.

The decision boundaries produced by an SVM and applied to a UT-7_{EPO} sample are shown in Figure 2(c). Comparison of the RBFP and the SVM decision boundaries show that application of either algorithm produced similar results. The SVM error estimation metrics are included as the last row in Table 2, and are similar to the top three performing ANNs.

As a final check on the applicability of an ANN system for classifying flow data, we applied the RBFP to the complete set of UT-7_{EPO} data for viability classification. Figure 2(d) shows the percentage of events by viability as a function of rhEPO dose, with the percent of live events dropping from greater than 90% to just over 40% with decreasing dosages of rhEPO. These results agree with the observation that starving UT-7_{EPO} cells for rhEPO induces apoptosis and cell death, and that replenishing with rhEPO rescues the cells in a concentration dependent manner (23).

The RBFP was then applied to an in vivo study designed to test the hypothesis that EPO inhibits apoptosis and cell death in erythroid precursor cells. The network classified events by viability and by lineage/developmental stage. Figure 4(a) shows the result of modeling the TER-119 and CD71 parameters using the EM algorithm. A well separated positive and negative population was visible for both parameters. In Figure 4(a), the left-hand box depicts the training ranges for nonerythroid (NE) events, the upper right-hand box depicts the ranges for late erythroid precursors (LPs), and the lower right-hand box depicts the ranges for very late erythroid precursors (VLPs). The EM algorithm result for modeling the 7AAD and annexin-V axes in vivo was similar to the in vitro result pictured in Figure 2(a). The resulting viability decision boundaries are shown in Figure 4(b). The expected error and percent varying performance metrics were calculated as a quality check, and were 2.1% $\pm$ 0.8% and 2.8%, respectively.

All events in the thirty-two sample in vivo data set were then classified with the RBFP networks and event counts were made of each population. Treatment with rhEPO reduced the fraction of live LPs in the marrow at 1 and 2 days to 68% $\pm$ 11% and 51% $\pm$ 7% of the control fraction respectively, as shown in Figure 4(c). The fraction of live LPs in the bone marrow returned to over 90% of the control fraction by 4 days. The fraction of live VLPs in the bone marrow steadily increased to 149% $\pm$ 20% of the control fraction at day eight, also shown in Figure 4(c). Overall there was an increase in erythroid lineage events in the bone marrow of all viability classes to 119% $\pm$ 7% of the control fraction after 8 days. Examination of the fraction of events in each viability class by lineage revealed that there was a significant increase in the fraction of dead LPs that reached a maximum at 2 days at 510% $\pm$ 48% of the control fraction, a corresponding significant decrease in live LPs to 68% $\pm$ 11% the control fraction, while the percentage of apoptotic LPs remained constant. These results are shown in Figure 4(d). There was no change in relative VLP composition by viability.

Discussion

We have developed a method of using ANNs to classify events from flow cytometric data using an in vitro viability study. The technique was then used to classify flow cytometric data by viability and lineage/developmental stage in an in vitro study designed to test the hypothesis that rhEPO increases the number of erythroid cells primarily by directly preventing apoptosis and cell death. This hypothesis is widely accepted and describes in part the control of apoptosis, a critical biological system (34,35). The results of this study have caused us to reject this hypothesis and to consider that rhEPO may have a more complicated in vivo mechanism of action.

We chose to apply pattern recognition techniques to flow cytometric data to develop objective criteria and to analyze data with more than two relevant parameters. Previously applied pattern recognition methods did not accommodate our desire to classify in vivo cells with regard to biological relevancy. The work of Roederer et al. (36–38) uses statistical tests on distributions of flow data to explore differences between control and test populations. Boddy et al. have applied ANNs to classify phytoplankton (39), but was able to select training examples and validate results in situ. It was thus necessary to develop an alternative algorithmic method. ANNs were chosen due to the precedent set by Body et al. and the existence of several recent studies (2–11) that contained some regions of 7AAD and annexin V intensity with consensus viability definitions. An in vitro data study using UT-7_{EPO} cells was used to develop our technique, and the RBFP was identified as the ANN best suited for this data based on an array of performance indices (Table 2). Similar decision boundaries (Figs. 2(b,c)) were found when an alternate pattern recognition technique, a support vector machine, was used to classify the data. Finally, classification of the UT-7_{EPO} data with the RBFP produced a dose dependent rescue of cells from apopto-

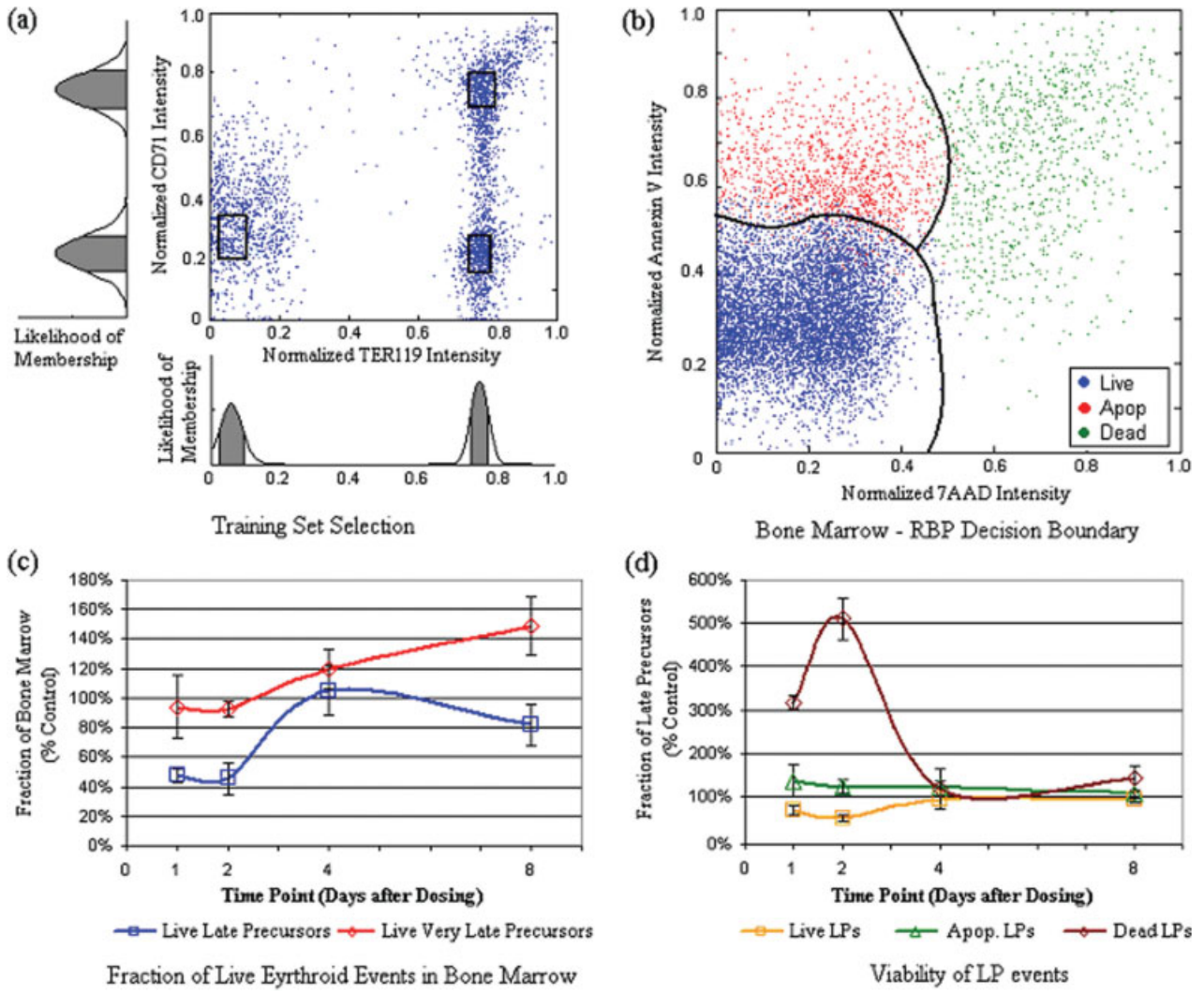

Figure 4. Time course results of in vivo study on the affects of rhEPO on apoptosis. (**a**) Result of the training data selection process for classifying cells by lineage and developmental stage. Example data is shown with models of the TER-119 and CD71 axes below and to the left respectively. In the example data, overlaid rectangles indicate the data selected for training. The rectangle in the lower left-hand corner marks the training set for nonerythroid precursors. The upper right-hand rectangle marks the LP precursors, and the lower right-hand rectangle marks the VLPs. (**b**) A two-dimensional projection of the viability decision boundary created by the RBFP for the in vivo data. (**c**) RBFP classification results; developmental stage of the live erythroid cells in the bone marrow, control versus rhEPO treated. At 1 and 2 days, we observe a decrease in the percentage of early erythroid precursors with rhEPO treatment. At 4 days, the percentage of LPs returned to baseline level. The percentage of VLPs increased consistently with rhEPO treatment. (**d**) Viability of LPs. We observe relatively constant viability proportions in the control samples. The rhEPO treated samples show a sharp increase in percentage of dead cells and a corresponding decrease in the percentage of live cells through 2 days. The percentage of apoptotic cells in rhEPO treated mice remained relatively constant.

sis and death (Fig. 2(d)), indicating that RBFP application may be an appropriate method for classification of flow cytometric data because these findings agree with the in vitro literature (23). The greatest challenge we face in this work was determining what metrics could be used to assess the success of the classifiers. With ground truth either difficult or impossible to ascertain regarding the class of the cells involved, we have used the metrics presented here. A possibility for future work would be to examine the work of Mackey, who has described alternate technologies for live cell classification, and Wong whose lab has produced several papers on phenotypic analysis of live cells (40–43).

The hypothesis that EPO primarily rescues cells from apoptosis and death can be studied by the application of the RBFP to in vivo data. We found that rhEPO caused an overall expansion of erythroid precursors as expected. However, a transient decrease in the percentage of live LPs with treatment was also observed, which was unexpected as LPs are thought to be among the erythroid precursors with the greatest concentration of EPO-receptor (34,35), and are

therefore expected to respond to rhEPO as hypothesized. When comparing control to rhEPO treated cells it is apparent that there is a transient decrease in live LPs and a corresponding increase in dead LPs with treatment, without a change in the percentage of apoptotic LPs (Fig. 4(d)). The VLPs showed a steady increase in the overall count without a change in relative proportion (Fig. 4(c)). It appears that the mechanism of EPO action may not be a rescue from apoptosis and cell death as hypothesized since the percentage of apoptotic cells remained unchanged in both erythroid precursor populations, and there was actually an increase in the percentage of dead LPs at 1 and 2 days. The mice received only the single dose of rhEPO during this 8 day trial, which implies that there may have been a transient increase in apoptotic cells prior to the first measured time point, leading to the noted increase in dead cells. We must thus reject our hypothesis and consider the possibility that EPO is involved in a more complicated regulatory process. Apoptosis has been shown to be an important regulatory mechanism in erythropoesis (Bugelski PJ, Nesspor T, O'Brien J, Makropoulos D, Shamberger K, Fisher PW, James I, Capocasale RJ. 2005. Pharmacodynamics of recombinant human erythropoietin in normal mice: Effects of a single dose on cell cycle, apoptosis and maturation of late stage erythroid precursors. Manuscript submitted for publication) and the fate of any given erythroid precursor is likely the result of an interplay of such factors as the density of EPO-receptor on the cells and the concentration of EPO (44) and expression of pro and antiapoptotic factors by erythroid precursors, e.g., TNF-α, TRAIL, Fas, Fas ligand, and Bcl-x (45–49).

To summarize, we have used a radial basis function perceptron to classify cells by viability and lineage/developmental stage, chosen based on metrics derived from specially selected test data, and have demonstrated the system is applicable to flow data. We used this technique to reject our study hypothesis that there is a simple mode of action for EPO stimulating the production of late stage erythroid precursors in anemia of chronic disease.

Literature Cited

1. Bohm I, Schild H. Apoptosis: The complex scenario for a silent cell death. Mol Imaging Biol 2003;5:2–14.
2. Korostoff J, Wang J, Kierba I, Miller M, Shenker B, Lally E. Actinobacillus actinomycetemcomitans leukotoxin induces apoptosis in HL-60 Cells. Infect Immun 1998;66:4474–4483.
3. Aubry JP, Blaecke A, Lecoanet-Henchoz S, Jeannin P, Herbault N, Caron G, Moine V, Bonnefoy JY. Annexin V used for measuring apoptosis in the early events of cellular cytotoxicity. Cytometry 1999; 37:197–204.
4. Derby E, Reddy V, Kopp W, Nelson E, Basler M, Sayers T, Malyguine A. Three-color flow cytometric assay for the study of the mechanisms of cell mediated cytotoxicity. Immunol Lett 2001;78:35–39.
5. Lecoeur H, Oliveira-Pinto L, Gougeon M. Multiparametric flow cytometric analysis of biochemical and functional events associated with apoptosis and oncosis using 7-aminoactinomycin D assay. J Immunol Methods 2002;265:81–96.
6. Lecoeur H, Février M, Garcia S, Riviére Y, Gougeon M. A novel flow cytometric assay for quantization and multi-parametric characterization of cell mediated cytotoxicity. Journal of Immunological Method 2001;253:177–187.
7. Lecoeur H, Ledru E, Prévost M, Gougeon M. Strategies for phenotyping apoptotic peripheral human lymphocytes comparing ISNT, annexin-V, and 7AAD cytofluorometric staining methods. J Immunol Methods 1997;209:111–123.
8. Philpott N, Turner A, Scopes J, Westby M, Marsh J, Gordon-Smith E, Dalgleish A, Gibson F. The use of 7 Amino Actinomycin D in identifying apoptosis: Simplicity of use and broad spectrum of application compared with other techniques. Blood 1996;6:2244–2251.
9. Telford G, Komoriya A, Packard B. Multiparametric analysis of apoptosis by flow and image cytometry. In: Hawley T, Hawley R, editors. Methods in Molecular Biology: Flow Cytometry Protocols, 2nd ed. Totowa: Human Press Inc.; 2004. pp 141–160.
10. Van der Pol M, Broxterman H, Westra G, Ossenkoppele G, Schuurhuis G. Novel multiparameter flow cytometry assay using Syto16 for the simultaneous detections of early apoptosis and apoptosis corrected P-glycoprotein function in clinical samples. Cytometry Part B 2003;55B:14–21.
11. Vermes I, Haanen C, Steffens-Nakken H, Reutelingsperger C. A novel assay for apoptosis flow cytometric detection of phosphatidylserine in early apoptotic cells using fluorescein labeled expression on Annexin V. J Immunol Methods 1995; 184:39–51.
12. Waters W, Harkins K, Wannemuehler M. Five color flow cytometric analysis of swine lymphocytes for detection of proliferation, apoptosis, viability and phenotype. Cytometry 2002;48:146–152.
13. King M, Radicchi-Mastroianni M, Wells J. There is substantial nuclear and cellular disintegration before detectable PS exposure during camptothecin-induced apoptosis of HL-60 cells. Cytometry 2000;40:10–18.
14. Socolovsky M, Constantinescu SN, Bergelson S, Sirotkin A, Lodish HF. Cytokines in hematopoiesis: Specificity and redundancy in receptor function. Adv Protein Chem 1999;52:141–198.
15. Chang K-H, Tam M, Stevenson MM. Inappropriately low reticulocytosis in severe malarial anemia correlates with suppression in the development of late erythroid precursors. Blood 2004;103:3727–3735.
16. Duda R, Hart P, Stork D. Pattern Classification. New York: Wiley; 2001. 654 p.
17. Kecman, V. Learning and Soft Computing: Support Vector Machines, Neural Networks and Fuzzy Logic Models. Cambridge: MIT Press; 2001. 541 p.
18. Elman J. Finding structure in time. Cogn Sci 1990;14:179–211.
19. Kohonen T. Self Organization and Associative Memory, 2nd ed. Berlin: Springer-Verlag; 1987. 501 p.
20. Rosenblatt F. Principles of Neurodynamics. Washington D.C.: Spartan; 1961.
21. Yee P, Haykin S. Regularized Radial Basis Function Networks: Theory and Application. New York: Wiley; 2001. 191 p.
22. Jain AK, Mao J, Mohiuddin KM. Artificial neural networks: A tutorial. Computer 1996;29:31–44.
23. Jelkmann W. The enigma of the metabolic fate of circulating erythropoietin (Epo) in view of the pharmacokinetics of the recombinant drugs rhEpo and NESP. Eur J Haematol 2002;69:265–274.
24. Keffer J, Probert L, Cazlaris H, Georgopoulos S, Kaslaris E, Kioussis D, Kollias G. Transgenic mice expressing human tumor necrosis factor: A predictive genetic model of arthritis. EMBO J 1991;10:4025–4031.
25. Capocasale RJ, O'Brien J, Makropoulos DA, Refferty P, Quinn J, Achuthanandam R, Kam M, Hrebien L, Bugelski P. Flow cytometric analysis of medullary hematopoiesis in tumor necrosis factor-α (Tg197) mice: A potential model of anemia of chronic disease. ASH 2003, San Diego, California, December 6–9, 2003.
26. Dempster A, Rubin D. Maximum likelihood from incomplete data via the EM algorithm. J R Stat Soc Ser B: Methodological 1977;39:1–38.
27. Watson J. Flow Cytometry Data Analysis. New York: Cambridge University Press; 1992. 288 p.
28. Kina T, Ikuta K, Takayama E, Wada K, Majumdar AS, Weissman IL, Katsura Y. The monoclonal antibody TER-119 recognizes a molecule associated with glycophorin A and specifically marks the late stages of murine erythroid lineage. Br J Haematol 2000;109:280–287.
29. Kohavi R. A study of cross-validation and bootstrap for accuracy estimation and model selection. Int Joint Conf Artif Intell 1995;2:1137–1145.
30. Webb A. Statistical Pattern Recognition. New York: Wiley; 2002. 496 p.
31. Toedling J, Rhein P, Ratei R, Karawajew L, Spang R. Automated in-silico detection of cell populations in flow cytometry readouts and its application to leukemia disease monitoring. BMC Bioinformatics 2006;7:282.
32. Rifkin R, Klautau A. In defense of one vs. all classification. J Machine Learn Res 2004;5:101–141.
33. Broomhead D, Lowe D. Multivariable functional interpolation and adaptive networks. Complex Syst 1988;2:321–335.
34. Fisher JW. Erythropoietin: Physiologic and pharmacologic aspects. Proc Soc Exp Biol Med 1997;216:358–369.
35. Fisher JW. Erythropoietin: Physiologic and pharmacology update. Proc Soc Exp Biol Med 2003;228:1–14.
36. Roederer M, Hardy R. Frequency difference gating: A multivariate method for identifying subsets that differ between samples. Cytometry 2001;45:56–64.
37. Roederer M, Treister AS, Moore W, Herzenber L. Probability binning comparison: A metric for quantitating univariate distribution differences. Cytometry 2001; 45:37–46.
38. Roederer M, Treister AS, Moore W, Hardy RR, Herzenber LA. Probability binning comparison: A metric for quantitating multivariate distribution differences. Cytometry 2001;45:47–55.
39. Boddy L, Morris CW, Wilkins MF, Al-Haddad L, Tarran GA, Jonker RR, Burkill PH. Identification of 72 phytoplankton species by radial basis function neural network analysis of flow cytometric data. Mar Ecol Prog Ser 2000;195:47–59.
40. Coskun H, Li Y, Mackey MA. Ameboid cell motility: A model and inverse problem, with an application to live cell imaging data. J Theor Biol 2007;244:169–179.
41. Yang F, Mackey MA, Ianzini F, Gallardo G, Sonka M. Cell segmentation, tracking, and mitosis detection using temporal context. Med Image Comput Assist Interv Int Conf Med Image Comput Comput Assist Interv 2005;8 (Part 1): 302–309.

42. MacLean JA, Su Z, Guo Y, Sy MS, Colvin RB, Wong JT. Anti-CD3:anti-IL-2 receptor bispecific monoclonal antibody. Targeting of activated T cells in vitro. J Immunol 1993;150:1619–1628.
43. MacLean JA, Su Z, Colvin RB, Wong JT. Anti-CD3:anti-IL-2 receptor-bispecific mAb-mediated immunomodulation. Low systemic toxicity, differential effect on lymphoid tissue, and inhibition of cell-mediated hypersensitivity. J Immunol 1995; 155:3674–3682.
44. Testa U. Apoptotic mechanisms in the control of erythropoiesis. Leukemia 2004;18: 1176–1199.
45. Kelley LL, Koury MJ, Bondurant MC, Koury ST, Sawyer ST, Wickrema A. Survival or death of individual proerythroblasts results from differing erythropoietin sensitivities: A mechanism for controlled rates of erythrocyte production. Blood 1993;82:2340–2352.
46. Jacobs-Helber SM, Roh K-H, Bailey D, Dessypris EN, Ryan JJ, Chen J, Wickrema A, Barber DL, Dent P, Sawyer ST. Tumor necrosis-alpha expressed constitutively in erythroid cells or induced by erythropoietin has negative and stimulatory roles in normal erythropoiesis and erythroleukemia. Blood 2003;101: 524–531.
47. Zamai L, Secchiero P, Pierpaoli S, Bassini A, Papa S, Alnemri E, Guidotti L, Vitale M, Zauli G. TNF-related apoptosis-inducing ligand (TRAIL) as a negative regulator of normal human erythropoiesis. Blood 2000;95:3716–3724.
48. Silva M, Richard C, Benito A, Sanz C, Olalla I, Fernandez-Luna JL. Expression of Bcl-x in erythroid precursors from patients with polycythemia vera. N Eng J Med 1998;338:564–571.
49. Stahnke K, Hecker S, Kohne E, Debatin KM. CD95 (APO-1/FAS)-mediated apoptosis in cytokine-activated hematopoietic cells. Exp Hematol 1998;26:844–850.